A&A 387, 507–519 (2002)
DOI: 10.1051/0004-6361:20020304

Astronomy & Astrophysics

Asymptotic Giant Branch evolution at varying surface C/O ratio: effects of changes in molecular opacities

P. Marigo⋆

Dipartimento di Astronomia, Università di Padova, Vicolo dell'Osservatorio 2, 35122 Padova, Italia

Received 21 December 2001 / Accepted 27 February 2002

Abstract. We investigate the effects of molecular opacities on the evolution of TP-AGB stars that experience the third dredge-up, i.e. with surface abundances of carbon and oxygen varying with time. To this aim, a routine is constructed to derive the molecular concentrations through dissociation equilibrium calculations, and estimate the opacities due to H_2, H_2O, OH, C_2, CN, and CO for any given density, temperature and chemical composition of the gas. Then, synthetic TP-AGB models with dredge-up are calculated by either adopting the newly developed routine, or interpolating between fixed opacity tables for solar chemical composition. The comparison between the two cases shows that the change in the dominant opacity sources, as the C/O ratio grows from below to above unity, crucially affects the evolution of the effective temperature, i.e. causing a notable cooling of the carbon-rich models (with C/O$>$ 1). From the comparison with observational data, it turns out that TP-AGB models with variable molecular opacities are able to reproduce the observed range of effective temperatures, mass-loss rates, and wind expansion velocities of C-type giants in the solar neighbourhood, otherwise failed if assuming fixed molecular opacities for solar-scaled mixtures. Finally, we mention other possibly important evolutionary and observational effects that result from the adoption of the variable opacities, such as: i) significant shortening of the C-star phase due to the earlier onset of the super-wind; ii) consequent reduction of the carbon yields; iii) reproduction of the observed range of near-infrared colours of C-stars.

Key words. stars: AGB and post-AGB – stars: evolution – stars: carbon – stars: fundamental parameters – stars: mass loss

1. Introduction

The spectra of cool giant stars – with spectral types M-S-C – are dominated by totally different molecular absorption bands in the visual and infrared (e.g. Lançon & Wood 2000) depending on which, carbon or oxygen, is the most abundant element. For instance, oxygen-rich stars exhibit strong bands of TiO, VO, H_2O, whereas carbon-rich stars show large absorption features of C_2, CN, SiC. These striking spectral differences between oxygen-rich and carbon-rich stars were first quantitatively explained by Russell (1934), on the basis of molecular equilibria calculations. The key-point is that the binding energy of the CO molecule is so high that almost all atoms of the least abundant element – C or O – are locked to form CO, while the excess atoms of the most abundant element are involved in the formation of the characteristic molecular bands. In addition, the relative abundances of carbon and oxygen affect the chemical composition of the predominant dust grains – e.g. amorphous silicates in oxygen-rich mixtures, and amorphous carbon grains in carbon-rich mixtures (see e.g. Ivezić & Elitzur 1995; Habing 1996) – which condensate in thick circumstellar envelopes ejected by AGB mass-losing stars.

These spectral differences in molecular blanketing and dust emissivity concur to create an observed sharp dichotomy in infrared colours between M- and C-type stars. For instance, the near-infrared colours (e.g. in the JHK bands) of carbon stars are systematically redder than those of oxygen-rich stars, as illustrated in several photometric surveys of AGB stars, e.g. in the Magellanic Clouds such as in Frogel et al. (1990), Costa & Frogel (1996), Sergei & Weinberg (2000, the 2MASS project), Cioni et al. (2000, the DENIS project). An analogous situation occurs in the far-infrared, e.g. in the IRAS two-colour diagram carbon-rich stars are displaced to larger [25−60] colours compared to oxygen-rich stars (see e.g. van der Veen & Habing 1988).

It is clear that theory should account for these observational features, also in consideration of the fact that huge amounts of infrared data are being released (e.g. the DENIS and 2MASS projects).

Actually, on the theoretical side the situation is as follows. The importance of molecular opacities in determining the photospheric properties of AGB stars

⋆ e-mail: marigo@pd.astro.it

has been demonstrated since long ago (e.g. Tsuji 1966). Depending on the surface C/O ratio, the dominant sources of opacities at low temperatures are different, being essentially those of H_2O and TiO for oxygen-rich atmospheres, and CN and C_2 for carbon-rich atmospheres (see e.g. the reviews by Gustafsson & Jørgensen 1994; Gustafsson 1995).

On one side, sophisticated model atmospheres for late-type stars have been constructed with the inclusion of molecular opacity data which are suitable for either M-type stars (e.g. Brown et al. 1989; Plez 1992; Bessell et al. 1998), or C-type stars (e.g. Querci et al. 1974; Johnson 1982; Jørgensen et al. 1992; Höfner et al. 1998).

On the other side, in most stellar evolution models of AGB stars the description of low-temperature opacities is still inadequate. In fact, the usually adopted prescriptions (e.g. Alexander & Ferguson 1994) correspond to opacity tables which are strictly valid for gas mixtures with solar-scaled abundances of elements heavier than helium, hence implying C/O $\sim$ 0.48. For a given initial metal content, the gas opacities are usually derived by interpolating the data tables as a function of density, temperature and hydrogen abundance. This means that any change in the true molecular opacities, due to e.g. variations of the surface CNO abundances, is neglected. The most notable drawback is that molecular opacities strictly valid for oxygen-rich configurations (with C/O < 1) are applied even to carbon-enriched models (with C/O > 1), regardless of the sharp dichotomy in the molecular equilibria between the two cases.

To our knowledge, limited sets of molecular opacity tables at variable C/O ratios are available in the literature (Alexander et al. 1983; Lucy et al. 1986), and few works are dedicated so far to consistently couple molecular abundances and opacities in evolutionary calculations of carbon stars. Scalo & Ulrich (1975) first calculate two AGB evolutionary sequences with variable molecular opacities. The effective temperatures of the models – with increasing surface carbon abundance – are derived with the aid of envelope integrations in which the molecular concentrations and relative low-temperature opacities are let vary according to the current CNO abundances. It turns out that the transition from C/O < 1 to C/O > 1 is marked by a significant cooling of the H-R tracks, essentially triggered by the sudden increase of the CN abundance and opacity. The sensitiveness to molecular opacities of the Hayashi limits for carbon stars has also been investigated by Lucy et al. (1986), in view of analysing the development of dust-driven winds at low effective temperatures. Finally, it is worth mentioning the work by Bessell et al. (1989, 1991) who present an analytical fit – as a function of the C and O abundances – to the molecular opacity calculations by Alexander et al. (1983).

In this context, the present study attempts to give a more realistic description of molecular opacities and discuss their effect on AGB evolution models. The work is organised as follows. The adopted procedure to calculate the opacities is described in Sect. 2. It closely resembles that

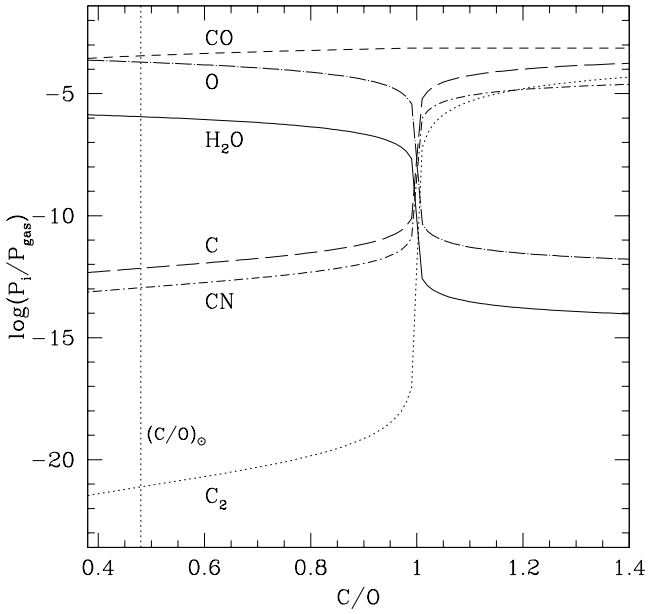

Fig. 1. Relative partial pressures of a few atomic and molecular species as a function of the C/O ratio, assuming a gas pressure $P_{\rm gas} = 10^3$ dyne cm^{-2}, and a temperature $T = 2500$ K. The vertical line intercepts the predicted molecular concentrations for a solar-like composition with C/O $\sim$ 0.48. Note the sharp dichotomy as C/O increases from below to above unity, for all species shown except the CO molecule. In fact, due to its high binding energy, the CO molecule always locks most atoms of the least abundant element between C and O.

developed by Scalo & Ulrich (1975): The mass absorption coefficient in any given point across the atmosphere is calculated with aid of analytical fitting relations, once the molecular concentrations are singled out with dissociation equilibrium calculations (Sect. 2.1). Our predictions are tested by comparison with detailed opacity calculations (Sect. 2.2) for solar-scaled elemental abundances, and also examined as a function of increasing carbon abundance and C/O ratio (Sect. 2.3).

The newly developed opacity routine is then employed in synthetic TP-AGB evolution calculations that include the effects of mass loss and third dredge-up (Sect. 3). The effective temperatures of the models, derived through envelope integrations, are analysed as a function of the C/O ratio as the evolution proceeds from oxygen-rich to carbon-rich configurations. The results obtained with "chemically-variable" opacities are compared with models based on "chemically-fixed" opacities, as well as with observations of M- and C-type giants in the solar neighbourhood (Sect. 3).

Other possible evolutionary effects produced by the improved opacities are discussed (Sect. 5), e.g. with respect to the C-star phase lifetimes, mass-loss rates, wind expansion velocities, surface carbon abundances and yields. We also mention further related improvements in the predictive capability of the models, i.e. to reproduce and discriminate the near-infrared colours of M- and C-type stars.

Concluding comments are summarised in Sect. 6.

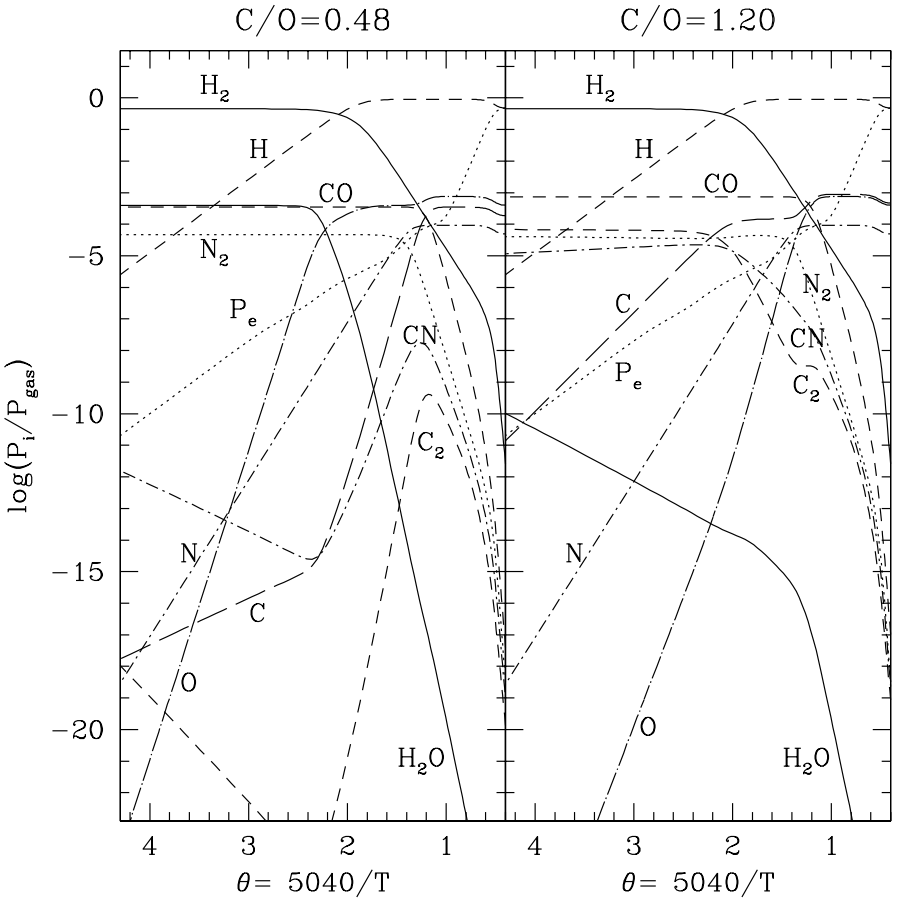

Fig. 2. Calculations of molecular dissociation and ionisation equilibria. The predicted evolution of the partial pressure for each species – relative to a fixed gas pressure $P_{\rm gas} = 10^3$ dyne cm^{-2} – is shown as a function of the temperature. $P_{\rm e}$ denotes the partial pressure due to free electrons. Two values of the C/O ratio are considered, i.e. the solar oxygen-rich configuration (left panel), and a carbon-rich configuration (right panel).

2. Opacity calculations

In order to get the gas opacities for whatever distribution of molecular species, we proceed as follows. The mass absorption coefficient κ (cm^2 gr^{-1}) is evaluated by adopting Keeley's (1970) analytical relations, which are parameterised as a function of gas density, temperature, and elemental abundances. These fitting formulas account for both atomic and molecular contributions to the total opacity. The molecules included by Keeley (1970) are: H_2, H_2O, OH, CO. The original H_2O term is modified to reproduce more recent opacity data (see Sect. 2.2). We add also the contribution of the CN opacity by adopting the polynomial fit by Scalo & Ulrich (1975). Finally, a rough estimate to C_2 opacity is given by simply assuming it as large as the CN term, following the results of detailed calculations by Querci et al. (1971; see their Fig. 11).

The functional form used to evaluate the total Rosseland mean opacity (RMO) is of the kind:

$$\kappa = \kappa_{\rm c} + \sum_i X_i \, \kappa_i \qquad (1)$$

where $\kappa_{\rm c}$ is the continuum opacity (due to absorption and scattering), κ_i represents the RMO produced per unit mass of molecule i, having a fractional abundance (by mass) X_i.

Because the RMO is a harmonic (not arithmetic) mean, in general, the sum of single RMO contributions – as given by Eq. (1) – is not equal to the RM of the sum of monochromatic opacities. Nevertheless, these two determinations tend to converge to the same result in case one of the involved terms dominates the summation. Actually, this condition is usually met in AGB envelopes under most conditions, the main source for the total RMO being either the continuous, or H_2O, or CN contribution (see Scalo & Ulrich 1975 for a discussion; see also Alexander et al. 1983; Alexander & Ferguson 1994).

2.1. Molecular concentrations

The evaluation of κ with Eq. (1) requires the abundances X_i of the atoms and molecules under consideration are known. For given density, temperature, and chemical composition of the gas, atomic and molecular concentrations are derived by means of chemical equilibrium calculations, i.e. by solving the set of equations describing both ionisation (Saha) and molecular dissociation equilibria (see e.g. Tsuji (1966) for a description of the overall procedure).

The electron pressure $P_{\rm e}$ is calculated by considering the first ionisation stages of H, He, C, N, O, and most metals with nuclear charge Z going from 9 to 57 (the complete list is the same as in Alexander & Ferguson 1994). The partition functions for atoms are taken from Irwin (1981), and Sauval & Tatum (1984). Dissociation equilibrium constants are evaluated with the aid of the analytical expressions by Rossi & Maciel (1983).

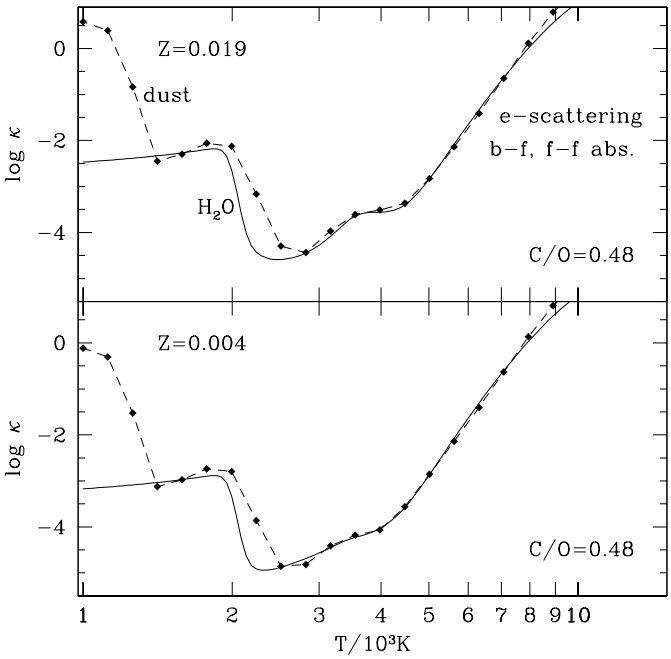

Fig. 3. Mass absorption coefficient (RMO) as a function of temperature, for two values of the initial metallicity as labelled. For each value of T, the corresponding density is derived from the condition $\log R = \log \rho + 3\,(6 - \log T) = -3$. The C/O ratio is assumed solar (0.48) in both cases. The results of the present work (solid lines) are compared to Alexander & Ferguson (1994) opacity calculations (dashed lines; the solid squares mark the actual points of available data tables, $R - T$ interpolation being adopted in between).

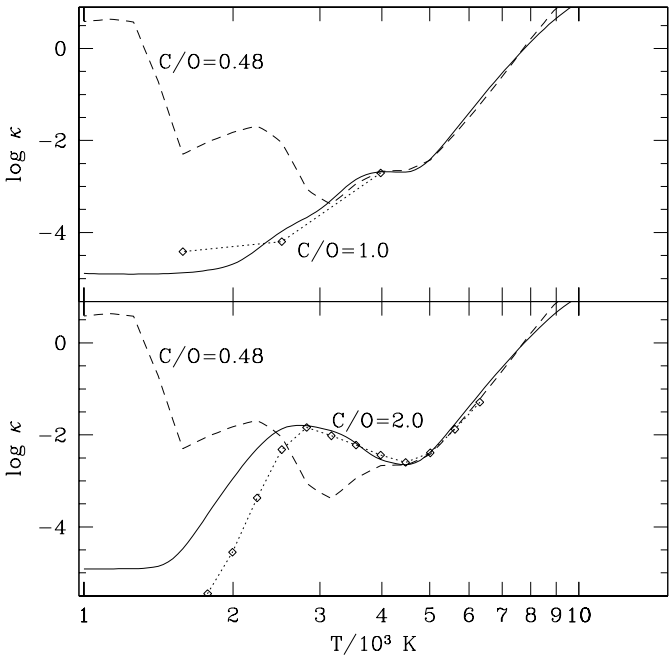

Fig. 4. Mass absorption coefficient (RMO) as a function of temperature, for different values of the C/O ratio as indicated. In all cases the density is assumed $\log \rho = -9$. The results of the present work (solid lines) are compared to detailed opacity calculations (dotted lines) by Alexander et al. (1983) for C/O = 1.0 (top panel), and Lucy et al. (1986) for C/O = 2.0 (bottom panel). The open squares along the curves mark the actual points of available data tables. For the sake of comparison, the opacity profile according to Alexander & Ferguson (1994) for C/O = 0.48 is also plotted (dashed line).

Figures 1 and 2 exemplify the results of standard calculations of chemical equilibrium, as a function of both C/O ratio and temperature. It is worth recalling the following points.

The stability of CO is so strong that, whatever the value of the C/O ratio, the majority of the atoms of the least abundant element is locked up in the CO molecule, whereas the excess of the other one can take part to the formation of other molecular species. This feature, pointed out long ago by Russell (1934), is responsible for the abrupt change in the atomic and molecular equilibria (involving C and O atoms) as soon as the gas mixture passes from oxygen-rich to carbon-rich (and vice versa).

A clear example is displayed in Fig. 1, where a remarkable increase of the fractional abundances (proportional to the partial pressures) of CN and C_2, and a consequent drop of H_2O, occur as soon as C/O become larger than unity. The same effect is evident by comparing the two panels of Fig. 2, that show the expected chemical equilibria as a function of temperature in a mixture with the same gas pressure, but two different values of the C/O ratio. We also notice that for temperatures lower than about 2000 K, the abundance of free H drops, as most H atoms are trapped into the H_2 molecule.

2.2. Comparison with other opacity data

The results of the present opacity calculations are tested by comparison with available data in the literature. In Fig. 3 the comparison is performed with Alexander & Ferguson (1994), whose opacity tables are largely adopted in current evolutionary calculations of the AGB phase (e.g. Chieffi et al. 2001; Herwig 2000; Ventura et al. 1999; Forestini & Charbonnel 1997). In these opacity tables the abundances of metals are scaled to the solar ones, then implying a C/O ratio of about 0.48 for any value of the metallicity. Figure 3 illustrates two examples, that refer to two choices of the initial composition, namely: [$Y = 0.273$, $Z = 0.019$] and [$Y = 0.240$, $Z = 0.004$]. In both cases, for each temperature value, the associated density satisfies the condition $\log R = \log \rho + 3\,(6 - \log T) = -3$, where R is a commonly adopted quantity as it allows smooth interpolations of opacity tables.

Our predictions in Fig. 3 show a general agreement with Alexander & Ferguson (1994), reproducing rather well the main features of the opacity for temperatures in the range from about 10 000 K down to about 1500 K. In particular, we account for the first opacity bump at $T \lesssim 2500$ K due to water vapor. To this respect, we should also note that, according to Alexander & Ferguson (1994), an additional smaller contribution to the opacity bump

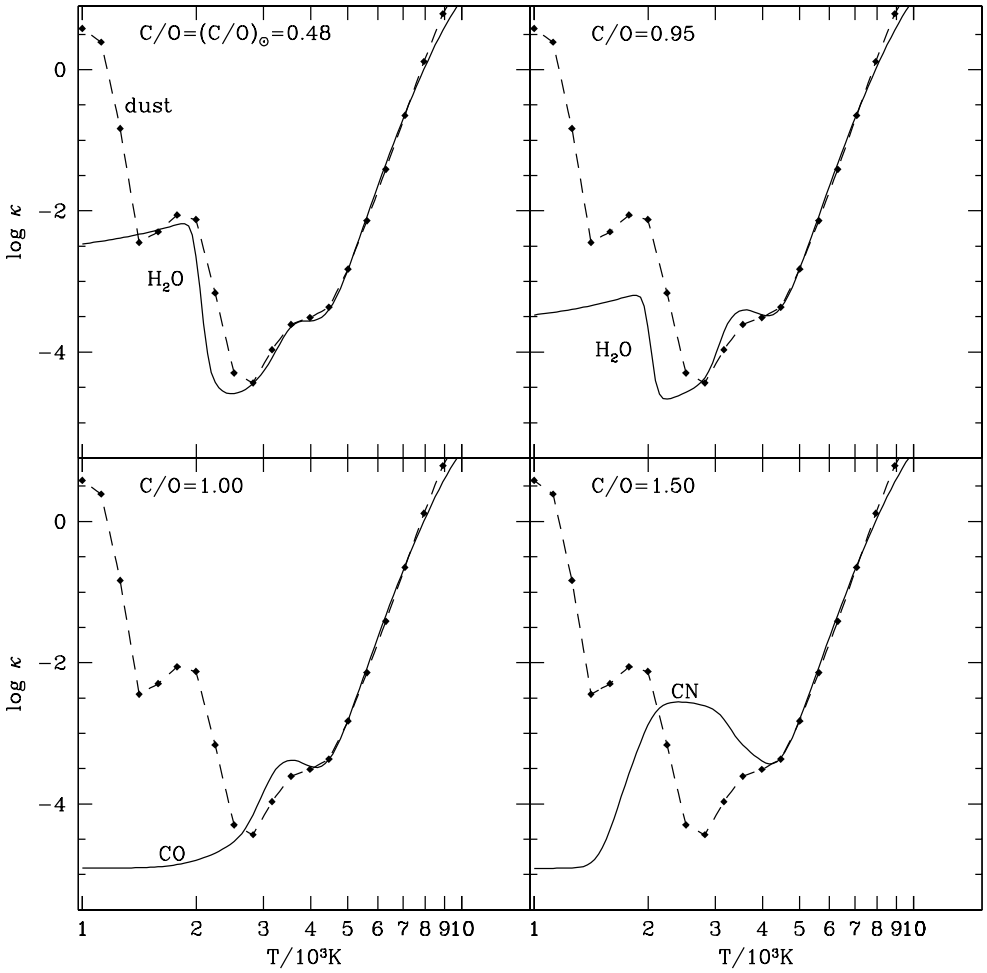

Fig. 5. The same as in Fig. 3, but for four different values of the C/O ratio, as indicated in each panel. The initial metallicity is $Z = 0.019$. Results of present calculations (solid lines) are always compared to Alexander & Ferguson (1994; dashed lines) predictions that refer to fixed solar C/O ratio. Dominant molecular contributions to the opacity are labelled nearby the corresponding parts of the curve. See text for further details.

comes from TiO, which is not included in the present treatment.

Anyhow, as the original (Keeley 1970) formula underestimates the H_2O opacity compared to Alexander & Ferguson's results, we choose to modify the corresponding analytical term k_{H_2O} in Eq. (1)[1], so as to obtain a better reproduction of the more recent opacity data. In fact, the water vapor opacity has been totally revised over the years, essentially following the introduction of new techniques and extension of the adopted line list (see e.g. Alexander et al. 1989; Gustafsson 1995).

The second opacity bump for $T < 1500$ is not reproduced by our calculations as the dust contribution is not taken into account. However, these very low temperature are not attained in the atmospheres of our carbon star models.

Figure 4 compares our results with available opacity data for gas mixtures with C/O = 1 (Alexander et al. 1983), and C/O = 2 (Lucy et al. 1986). The oxygen abundance is kept solar, while that of carbon is increased so as to obtain the specified C/O ratio. We notice in both cases the opacity curves at $T < 4500$ K largely deviate from that corresponding to a solar-scaled mixture of metals (with C/O ~ 0.48) (see the discussion below in Sect. 2.3). The basic features – i.e. the disappearance of the H_2O opacity bump for C/O = 1 and the appearance of the CN opacity bump for C/O = 2 – present in the data tables are also predicted by our calculations. Some differences exist, like a possible overestimation of the CN opacity at temperatures lower than 2500 K (bottom panel of Fig. 4). Nevertheless, the results shown in Figs. 3 and 4 clearly show that our simple opacity treatment provides a satisfactory description of the behaviour of molecular opacities with varying C/O ratio, and represents a better alternative to the usual assumption of opacities for solar-scaled metal abundances.

2.3. Molecular opacities for variable C/O ratio

Figure 5 shows a striking example of how large might be the discrepancy between "chemically-fixed" and "chemically-variable" opacity data. The former case refers to a fixed solar-like composition according to Alexander & Ferguson (1994), whereas the latter case corresponds to a chemical mixture with increasing C abundance.

We can see that major variations of the opacity show up as the C/O ratio increases from below to above unity (due to the progressive increase of the C abundance). At lower temperatures ($T \lesssim 3000$ K) the H_2O bump drops

[1] More specifically, the numerator $9.72 \times 10^{-18} e^{-3.2553/T_4}$ has been replaced with $9.72 \times 10^{-21} e^{-3.2553/(T_4+0.37)}$, where $T_4 = T/10^4$ K.

until it disappears at C/O $\sim$ 1, as almost all atoms of both C and O are bound in the CO molecule. Then, as soon as C/O overcomes unity, the CN+C_2 opacity contribution suddenly rises, becoming the dominant opacity source at temperatures between 2000 and 3000 K. It turns out that such a prominent opacity bump develops just where an opacity minimum is instead expected for oxygen-rich mixtures.

Therefore, by comparing the results displayed in Fig. 5, it is already clear that applying the opacity profile expected for a solar mixture to calculate the atmosphere of a carbon-rich model is a considerable mismatch. However, this is presently the usual choice in stellar evolution calculations of the AGB phase.

2.4. Pros and cons of the present opacity treatment

A few comments should be made with respect to the pros and cons of the present treatment. A clear limitation is related to the adopted simplifications, namely: calculate κ as the sum of RMOs of individual molecules, and include a limited number of molecular species. However, we already mentioned that Eq. (1) may be considered an acceptable approximation under most conditions met in AGB atmospheres. Possibly important molecules in AGB stars, that are neglected in this study, are TiO and VO for oxygen-rich stars and HCN and C_2H_2 for carbon-rich stars. Anyhow, the molecules here considered are among the most relevant opacity sources at low temperatures in AGB stars.

The major advantage is offered by the possibility to evaluate the opacities for *any* chemical composition, *during* the evolutionary calculations, and with just a small additional computational effort.

Clearly, a more accurate alternative would be to perform multidimensional interpolations between tables previously generated by detailed opacity calculations. However, it should be remarked that in order to guarantee a sufficient coverage of the possible conditions met in AGB atmospheres, a large grid of tables is needed (and presently not available), for many combinations of various parameters. In the specific case of AGB stars, we should deal with a minimum of seven parameters, namely: density, temperature, total metal content, hydrogen, carbon, nitrogen, and oxygen abundances.

It follows that, despite the involved approximations, our approach is a reasonable compromise and also an improvement upon commonly adopted input prescriptions in AGB evolution models (i.e. solar-scaled molecular opacities), as it can describe the changes in the atmospheric opacities consequent to the changes in the surface chemical composition of AGB stars.

3. Synthetic TP-AGB calculations

The new routine to evaluate the molecular opacities, described in Sect. 2, is incorporated in the envelope model employed in the code for synthetic TP-AGB evolution developed by Marigo et al. (1996, 1998) and Marigo (2001, and references therein), to whom the reader is referred for all details.

Let us here summarise just the basic structure of the TP-AGB synthetic model. It consists of two main components, namely:

- analytical ingredients derived from full stellar calculations and/or observations (e.g. core mass-luminosity relation for low-mass stars, core mass-interpulse period relation, mass-loss and dredge-up laws, etc.);
- a complete "extended" envelope model that, at each time step, numerically solves the structure of the stellar atmosphere and underlying convective envelope, down to the H-burning shell.

As for the envelope model, the solution scheme is the following. Given total stellar mass, core mass, and surface chemical composition, the stellar structure equations are integrated to determine the profile of the unknown variables r, P_r, T_r, L_r across the envelope, provided that two outer (at the photosphere) and two inner (at the core) boundary conditions are fulfilled. In particular, the outer boundary conditions – derived from the integration of the photospheric equations for T and P – are related to the atmospheric parameters L and $T_{\rm eff}$. Static and grey atmospheres are assumed. Convection is described according to the mixing-length (ML) theory, and the ML parameter is $\alpha = \Lambda/H_{\rm P} = 1.68$ (where Λ is the mixing length, and $H_{\rm P}$ is the pressure-scale height).

Envelope integrations are carried out to predict the evolution of the envelope structure and surface properties of a TP-AGB star during the quiescent inter-pulse periods, that is when the H-burning shell provides most of the stellar energy, while the He-shell contribution is small. In terms of duration, this quiescent phase – between the occurrence of two consecutive thermal pulses – is by far dominant, given the extremely shorter time over which a thermal pulse takes place.

The envelope model is also employed to test the possible occurrence of the third dredge-up, according to a criterium on the temperature at the base of the convective envelope in the stage of post-flash luminosity maximum. The minimum base temperature required for dredge-up to take place is $\log T_{\rm b}^{\rm dred} = 6.4$, following the empirical calibration performed by Marigo et al. (1999; see also Wood 1981) on the basis of the observed carbon star luminosity functions in the Magellanic Clouds. The efficiency of the third dredge-up, expressed by the classical quantity λ, is a free parameter, that varies within 0.50–0.75 in the present calculations. The recurrent dredge-up of carbon at thermal pulses is responsible for the transition of the models from the (C/O $<$ 1) to the (C/O $>$ 1) domain. Hot-bottom burning (and the related break-down of the core mass-luminosity relation) in the most massive models (with $M \gtrsim 3{-}4\,M_{\odot}$) is also taken into account (Marigo et al. 1998; Marigo 1998). The TP-AGB evolution is calculated with the inclusion of mass loss up to the

complete ejection of the residual envelope. The adopted semi-empirical formalism for mass-loss is that developed by Vassiliadis & Wood (1993).

For the purposes of this study, a limited set of synthetic TP-AGB models has been calculated, with initial metallicity $Z = 0.019$ and masses in the range $1.2\,M_{\odot}$–$3\,M_{\odot}$. For each stellar model, calculations start at the first thermal pulse, following the predictions of the Padova stellar tracks (Girardi et al. 2000), whence we extract our initial conditions (i.e. core mass, envelope chemical composition, luminosity, etc.). In the TP-AGB models here considered, with relatively low masses, the surface chemical composition may be altered by the third dredge-up only, whereas hot-bottom burning does not take place.

As far as the adopted opacity prescriptions are concerned, we distinguish two groups of models. In both cases we take the tables by Iglesias & Rogers (1993) for $\log T > 4.0$, and Alexander & Ferguson (1994) for $3.7 < \log T \leq 4.0$. The only difference resides in the choice of the adopted opacities for $\log T \leq 3.7$:

- models F: fixed opacities for solar-scaled metal abundances
- models V: variable opacities (Sect. 2) coupled to the changes in chemical abundances (e.g. C and O) due to dredge-up events

In fact, these are the typical temperatures at which the molecular concentrations become appreciable (see e.g. Figs. 3–5).

4. Effective temperatures of oxygen- and carbon-rich stars

It has long been recognised that the opacity of the atmospheric layers plays a crucial role in determining the surface properties of giant stars, in particular affecting their position on the H-R diagram (e.g. Lucy et al. 1986). From stellar models we learn that for given luminosity (determined e.g. by the core mass-luminosity relation), larger atmospheric opacities usually correspond to larger radii, hence lower effective temperatures.

This may apply for instance, to a C-rich atmosphere compared to an O-rich atmosphere, if the typical range of involved temperatures across both atmospheres is (say between 2000 and 4000 K) is such to include important opacity features, like the CN opacity bump (or opacity minimum) of the C-rich (or O-rich) configuration (see Fig. 3). In this case, then, a cooler effective temperature should describe the C-rich model.

This prediction may explain, in fact, the existence of a clear relation between the effective temperatures of giant stars and their surface C/O ratios: Carbon-rich stars are found to have lower effective temperature than oxygen-rich stars. This trend is illustrated in Fig. 6, where the observed data refer to a sample of Galactic giants.

The effective temperatures of most carbon stars of the sample are the most accurate possible determinations, as they have been derived with the aid of *direct* methods, based on angular diameters estimated with interferometry or lunar occultations (see the compilation by Bergeat et al. (2001) and references therein). For the other stars (of M-type with C/O < 1 and SC-type with C/O ~ 1), effective temperatures are indirectly derived via spectral analysis techniques employed to determine their CNO abundances, hence C/O ratio (e.g. Smith & Lambert 1986).

The empirical relation shown in Fig. 6 clearly indicates two major facts, namely: i) the almost complete segregation in effective temperature between oxygen-rich and carbon-rich stars; and ii) the relatively low C/O values (< 2) measured in carbon-rich stars.

The observed data are then compared to the two sets (F and V) of TP-AGB synthetic models, that only differ in the adopted prescriptions for low-temperature opacities ($\log T < 3.7$).

Figure 6 shows the remarkable disagreement between observations and predictions for models F (bottom panel). The observed domain of C-stars is not reached by the stellar tracks, that are characterised by higher effective temperatures and larger C/O ratios. It should be also noticed that, as the surface C/O ratio increases because carbon is added at each dredge-up episode, the decrease of $\log T_{\rm eff}$ follows an almost straight line, up to when a more significant bending towards lower $T_{\rm eff}$ takes place during the very last quiescent inter-pulse periods. Actually, the slope of the C/O $-$ $\log T_{\rm eff}$ tracks does not change even when models F make the transition from C/O < 1 to C/O > 1. This can be understood just from the fact that in models F the molecular opacities are not affected at all by changes in the CNO abundances. The final flattening of tracks is instead caused by the drastic reduction of the envelope mass at the onset of the super-wind regime.

The effect of the new molecular opacities shows up sharply in models V. First of all, they succeed in reproducing the observed location of both oxygen- and carbon-rich stars, hence removing the aforementioned discrepancy. The main aspect is that, contrary to models F, models V with variable opacities perform quite a large excursion towards lower effective temperature as soon as their surface abundance of C exceeds that of O. Such excursion is initially driven by the sudden appearance and progressive build-up of the molecular opacities due to CN and C_2 (see Fig. 5) as the C/O ratio becomes larger than unity. The photospheric cooling, in turn, favours larger and larger mass-loss rates, contributing to anticipate the super-wind phase.

In brief, the behaviour of tracks F and V notably differs in the flattening towards lower $T_{\rm eff}$ shown in Fig. 6. In models F the bending is caused by the reduction of the envelope mass, and starts at the onset of the superwind *after* the transition to the C-rich class. In models V it is initiated by the drastic change in molecular opacities *as soon as* the oxygen- to carbon-rich transition occurs, and subsequently amplified during the super-wind phase. This feature can be seen also by looking at the TP-AGB evolution in the H-R diagram (see Fig. 7): compared to models F

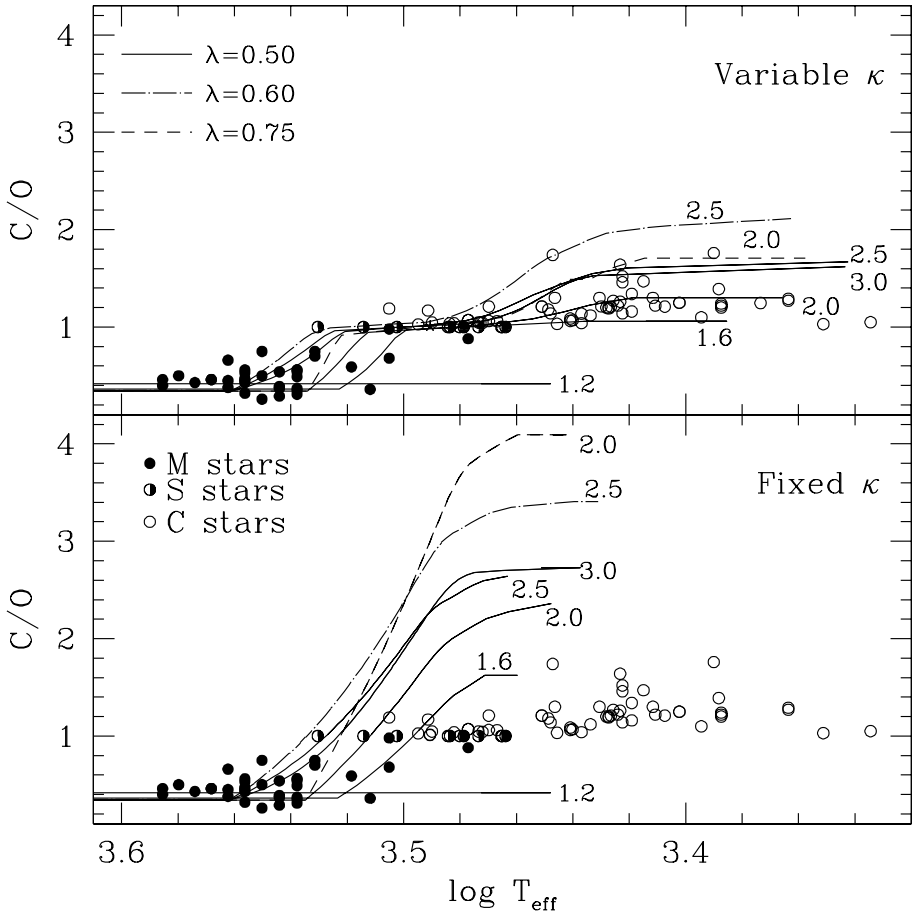

Fig. 6. Effective temperatures as a function of the C/O ratio in Galactic giants. Abundance determinations are taken from: Smith & Lambert (1985, 1986, 1990) for M stars (C/O $<$ 1); Ohnaka & Tsuji (1996) for S stars (C/O $\sim$ 1); Lambert et al. (1986), Ohnaka et al. (2000) for C stars (C/O $>$ 1). Effective temperatures are taken from the same quoted works, except the C-star group for which we refer to Bergeat et al. (2001; their Table 13). Observed data (circles) are compared to predictions of synthetic TP-AGB models with dredge-up (lines), adopting either "chemically-fixed" opacities (bottom panel), or "chemically-variable" opacities (top panel). See text for more details.

with the same initial mass, the flattening of tracks V occurs at fainter luminosities and extends to cooler $T_{\rm eff}$.

It is also interesting to notice that the transition to the C-star configuration is characterised by a first sizeable jump towards lower $T_{\rm eff}$ (compare the last C/O $<$ 1 point with the first C/O $>$ 1 point along each H-R track of group V), which is more pronounced at decreasing stellar mass. After this initial sharp departure away from the oxygen-rich part of the H-R track, the subsequent cooling proceeds at a slower rate during the C-star evolution, as illustrated by the denser sequence of points marked along tracks V in Fig. 7. Finally, a further acceleration towards lower $T_{\rm eff}$ takes place as soon as the super-wind is attained and the envelope is rapidly ejected (correspondingly, the distance in $T_{\rm eff}$ between the last points increases).

This predicted behaviour naturally succeeds in explaining the observed spread and distribution in effective temperature exhibited by the sample of M-S-C stars shown in Fig. 6. To this aim, let us consider the overall morphologic evolution of the bundle of theoretical TP-AGB tracks (models V, top panel).

For C/O $<$ 1 (corresponding to M-stars), the width in $T_{\rm eff}$ of the bundle is relatively narrow and reflects individual variations of fundamental parameters (essentially: envelope and core masses, and dredge-up law).

For C/O $\sim$ 1, at the M-to-C transition, the bundle stretches out over a rather extended $T_{\rm eff}$-interval, as a consequence of the expected jump shown by each track. This is fully supported by the observed location of S-stars in Fig. 6.

Finally, as the bundle widens for C/O $>$ 1, the evolution is characterised by a further significant cooling of the tracks, that depends on individual stellar properties (compare e.g. the tracks of the same stellar mass but with different λ). Indeed, models V are in agreement with the empirical indication, already pointed out by Bergeat et al. (2001), that the dispersion of the C/O values measured in C-stars increases at decreasing effective temperatures.

5. Other evolutionary and observational effects

In addition to the mentioned effects on the effective temperature, the use of opacity prescriptions properly coupled to the current CNO abundances, may bring along other evolutionary implications of great relevance.

Some indications are presented in Table 1 and Figs. 8, 9 that compare the predictions for some representative quantities of synthetic TP-AGB models calculated with the same input physics but for the molecular opacities (i.e. models F and V presented in Sect. 4).

First of all, we can notice in Table 1 that the introduction of the new opacities in our TP-AGB calculations has determined a sizeable reduction of the duration of the C-star phase, by a factor 2–3 for the specific models under consideration.

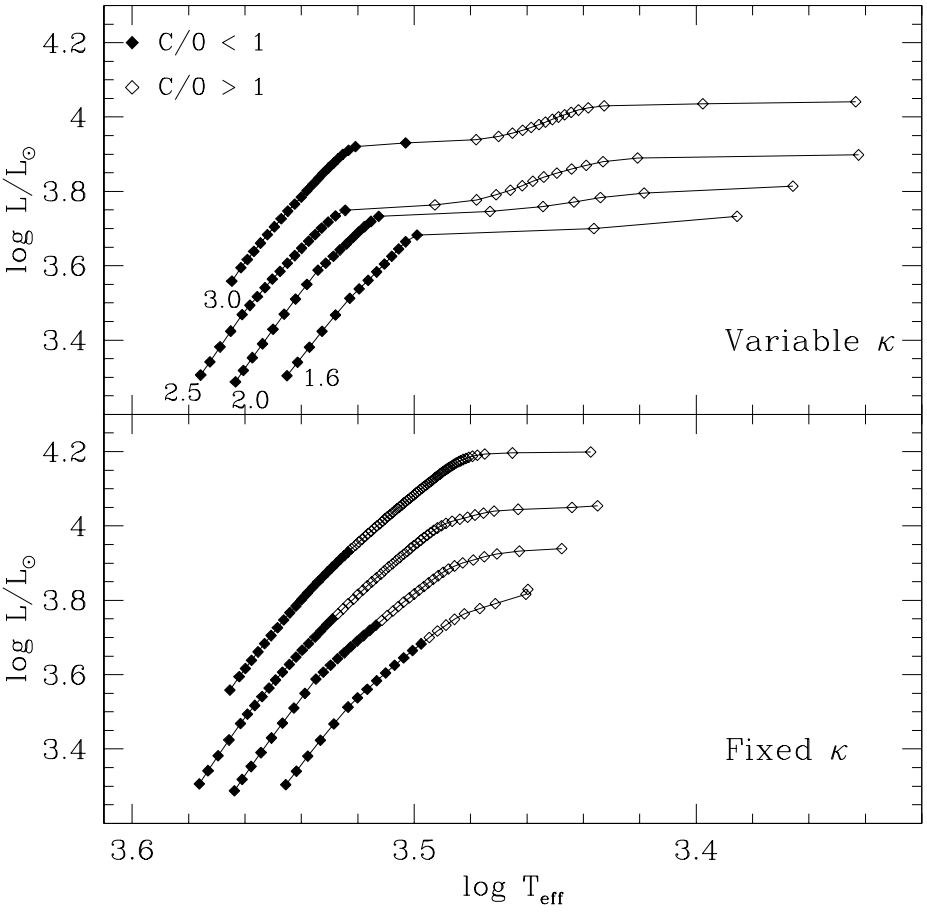

Fig. 7. Predicted H-R tracks of TP-AGB models with initial metallicity $Z = 0.019$. Calculations are carried out with both fixed (bottom panel) molecular opacities for solar composition, and variable opacities (top panel) related to the current photospheric abundances of C and O (hence C/O ratio) during the evolution. In all models the dredge-up efficiency is assumed $\lambda = 0.5$. Squares along the tracks mark the pre-flash luminosity maximum at the end of each pulse-cycle.

Table 1. Predictions of synthetic TP-AGB models calculated with fixed (F) molecular opacities for solar composition, and variable (V) molecular opacities. The assumed dredge-up efficiency parameter is $\lambda = 0.5$. From left to right the table entries correspond to: stellar initial mass; duration of the TP-AGB phase; duration of the C-star phase; mean effective temperature when the surface C/O ~ 1.1; and values of C/O, luminosity, and final mass at the termination of the AGB.

$M_{\rm i}/M_\odot$	$\tau_{\rm TP-AGB}/(10^6$ yr)		$\tau_{\rm C}/(10^6$ yr)		$\langle T_{\rm eff}\rangle$(C/O ~ 1.1)		$({\rm C/O})_{\rm f}$		$\log L_{\rm f}/L_\odot$		$M_{\rm f}/M_\odot$	
	F	V	F	V	F	V	F	V	F	V	F	V
1.6	1.94	1.46	0.71	0.23	3 102	—	1.62	1.06	3.829	3.746	0.596	0.577
2.0	3.37	2.41	1.48	0.51	3 228	2 830	2.36	1.30	3.939	3.814	0.632	0.588
2.5	3.67	2.69	1.92	0.94	3 341	2 972	2.64	1.67	4.054	3.907	0.686	0.621
3.0	2.91	1.92	1.67	0.68	3 311	2 929	2.73	1.62	4.209	4.048	0.780	0.685

As already mentioned, such effect is related to the excursion towards lower effective temperatures caused by the transition from C/O < 1 to C/O > 1. This, in turn, favours larger mass-loss rates, hence anticipating the onset of the super-wind regime and the consequent termination of the AGB phase.

Another consequent effect concerns the luminosities of C-stars and the final masses at the termination of the AGB. As shown in Fig. 7, the luminosity interval spanned by models V for C/O > 1 is much smaller than in models F with the same mass and assumed dredge-up efficiency. Correspondingly, the AGB-tip luminosities, $L_{\rm f}$, and the final masses, $M_{\rm f}$, are lower in models V than in models F (see Table 1). From inspection of Fig. 7 (top panel), one could speculate that a well-defined relation exists between the observed C-star luminosity and its initial mass, and hence the age of its parent population. Moreover, since models V leave the AGB phase earlier than models F, we might expect that the initial-final mass relation tends to flatten over the initial-mass interval pertaining to the C-stars' progenitors. Before drawing any conclusion on these issues, however, it is necessary to perform an empirical re-calibration of the other model parameters (e.g. dredge-up law) that also affect the predicted C-star luminosities and final masses. The basic observables to be reproduced are the C-star luminosity functions e.g. in the Magellanic Clouds, and the white-dwarf mass distribution, as done by Marigo et al. (1999).

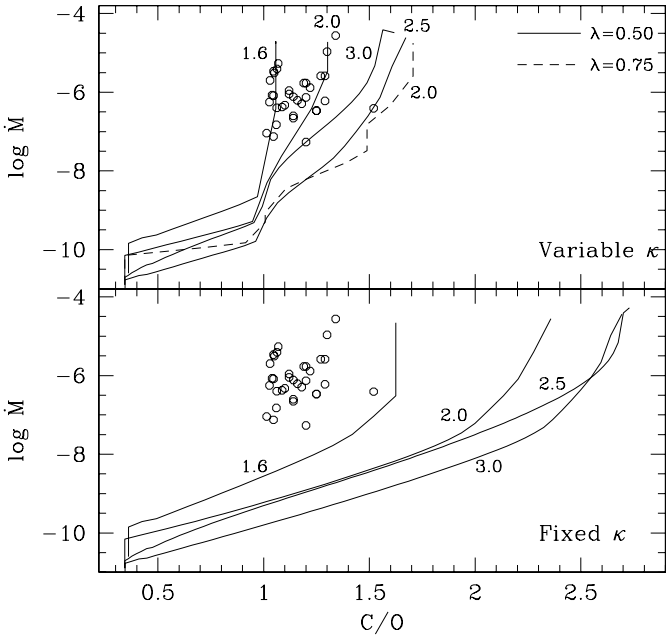

Fig. 8. Mass-loss rates on the AGB as a function of the surface C/O ratio. Observed data for carbon stars (circles) combine $\dot{M}$ determinations by Loup et al. (1993), and Wannier et al. (1990) with C/O ratio derived by Lambert et al. (1986), and Ohnaka et al. (2000). Theoretical tracks (lines) show the evolution of $\dot{M}$ as the surface C/O increases because of the third dredge-up. By comparing the top and bottom panels we can note how different are the predictions for the carbon-enriched models (with C/O > 1), depending on the molecular opacities adopted in envelope integrations.

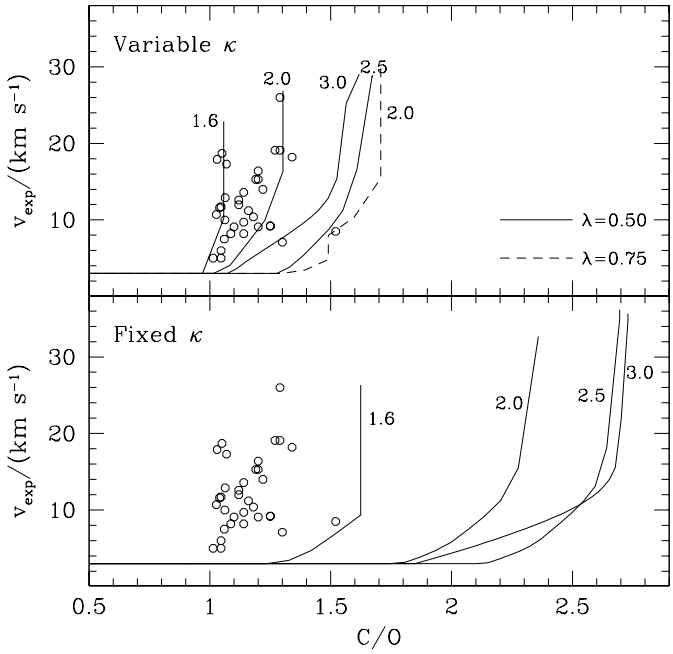

Fig. 9. Expansion velocities of AGB ejecta as a function of the surface C/O ratio. Observed data for carbon stars (circles) combine $v_{\rm exp}$ determinations by Loup et al. (1993) with C/O ratio derived by Lambert et al. (1986), Ohnaka et al. (2000). Theoretical tracks (lines) refer to the same sets of models as in Fig. 8.

With respect to mass loss on the AGB, we can see in Fig. 8 that models V describe the behaviour of the observed mass-loss rates of C-stars as a function of the C/O ratio remarkably well. Similarly to the H-R tracks, also the tracks V in the ($\dot{M}$ – C/O) plane show an evident change of slope as soon as surface carbon becomes more abundant than oxygen, with a clear acceleration towards larger and larger $\dot{M}$. Differently, in models F the change of slope is found to occur at the onset of the superwind, that is after the transition into the C/O > 1 domain. An analogous situation applies to the evolution of the terminal (or expansion) velocity, $v_{\rm exp}$, of the AGB wind as a function of the C/O ratio, which is shown in Fig. 9. It is calculated – following Vassiliadis & Wood's (1993) prescriptions – as a function of the pulsation period which, in turn, depends also on $T_{\rm eff}$. Again, models V are in much better agreement with observations of C-stars compared to models F, and again a sudden change of slope is seen at the C-star formation. All these features point to the same conclusion: the surface C/O ratio of AGB stars is a crucial factor in determining their evolutionary properties.

Further notable consequences arise from this ascertainment. For instance, the reduction of the C-star lifetimes (passing from models F to models V) consequently affects other model predictions regarding e.g. the expected $N({\rm C})/N({\rm M})$ ratio between the number of C- and M-stars in old- and intermediate-age stellar populations, the carbon abundances and yields. Basing on the results presented in Table 1, all these quantities show a decreasing trend going from models F to models V. For instance, the ratio $\tau_{\rm C}/(\tau_{\rm TP-AGB}-\tau_{\rm C})$ as a function of stellar mass is a measure of the expected $N({\rm C})/N({\rm M})$ ratio – limited to late M-stars – as a function of the age of the corresponding simple stellar population. According to present calculations, this ratio varies in the interval 0.58–1.35 for models F, and 0.19–0.55 for models V. Moreover, the interesting possibility of a lower production (and ejection) of carbon might help to explain the rather low C/H and C/O abundances measured in PNe, such as the accurate determinations recently derived from ISO spectra (Pottasch 2000). Actually, lower stellar yields of carbon seem also required by chemical evolution models of galaxies to better reproduce the observations (Portinari et al. 1998).

The improved treatment of molecular opacities should also allow a better description of near-infrared colours – mainly in the JHK bands – of AGB stars. Leaving a more detailed analysis of this topic to a future investigation, we briefly mention the observed dichotomy between oxygen- and carbon-rich stars in the $(J-K)$ vs. $(V-K)$ diagram. As shown in Fig. 10, M- and C-stars populate two different branches, the carbon-rich objects exhibiting systematically redder $(J-K)$ colours.

The predicted evolution of the colours is also shown for both sets of models. The transformations from the theoretical to the observational plane are performed by using the calibrated colour-temperature relations presented

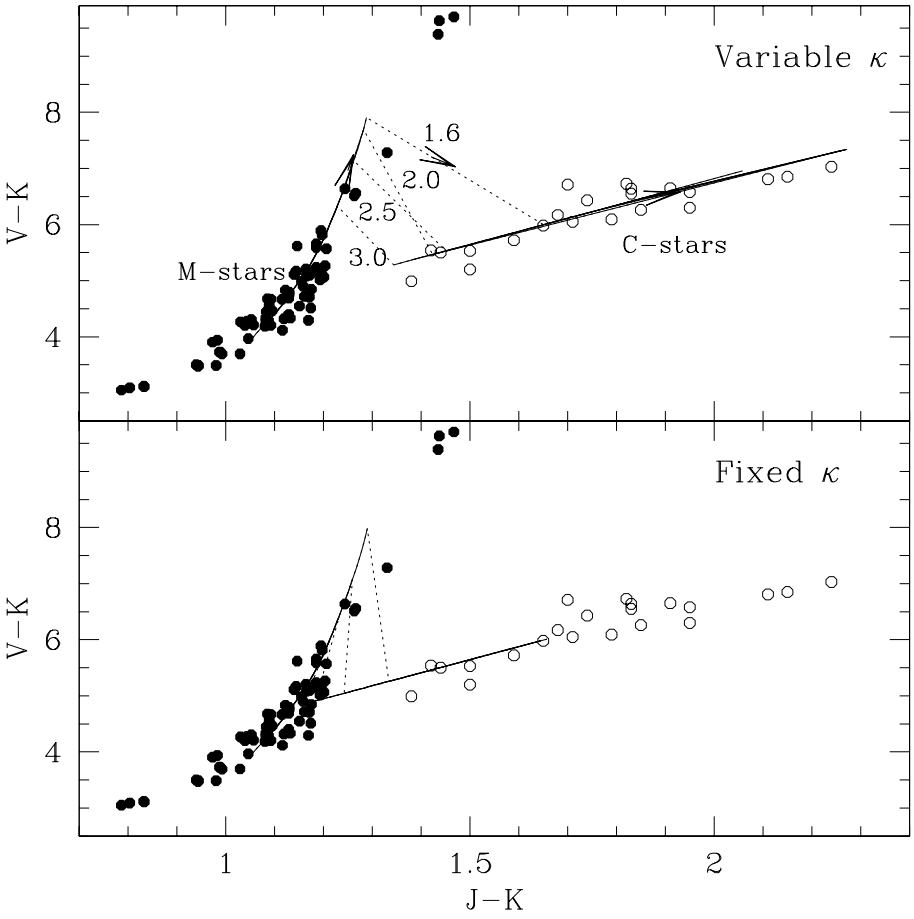

Fig. 10. Near-infrared colour-colour diagram for oxygen-rich (M-type) and carbon-rich (C-type) stars in the Solar neighbourhood. Observed data are taken from the compilations of M-stars by Fluks et al. (1994; filled circles), and C-stars by Bergeat et al. (2001, objects in their Table 4; empty circles). The predicted colour evolution on the TP-AGB is shown (solid lines, the direction is indicated by arrows) for different initial stellar masses (indicated in $M_{\odot}$), and fixed/variable molecular opacities. See text for more explanation.

by Fluks et al. (1994) for the M-stars, and Bergeat et al. (2001) for the C-stars. Combining the two transformations, an abrupt jump in both $(J-K)$ and $(V-K)$ colours is expected as soon as the stars pass from oxygen-rich to carbon-rich (dotted lines).

As for the C-star branch, we notice that models with variable opacities well extend throughout the observed range of the $(J-K)$, from about 1.3 up to about 2.2. Differently, carbon-rich models with fixed opacities get mixed into the M-star domain at lower colours (contrary to observations), and draw a shorter evolution towards redder colours, not exceeding $(J-K) \sim 1.7$.

It is clear that a deeper analysis of the results presented in this work requires extensive calculations of TP-AGB models, coupled to a close comparison with observations. It should be also considered that any further change in the input prescriptions – besides those for the molecular opacities – would produce additional effects. It follows that, in order to reproduce basic observational constraints (like the carbon star luminosity functions and the white dwarf mass distribution; see e.g. Marigo 2001), the adoption of the improved opacities should be accompanied by a re-calibration of the relevant model parameters (mainly dredge-up law and mass-loss efficiency). All these aspects will be considered with more detail in future work.

Anyhow, just from basing on the present explorative calculations, there is a clear hint that the new variable opacities go in the right direction to match theory and observations.

6. Concluding remarks

In this work we call attention to the importance of consistently coupling the molecular opacities with the current envelope chemical composition in TP-AGB evolution models, and to discontinue the use of opacity tables that are generated for fixed – both absolute and relative (usually solar-scaled) – abundances of metals, like carbon and oxygen.

Our explorative study starts with the development of a routine to estimate the molecular opacities for any choice of the chemical composition of the gas. Notwithstanding the unavoidable approximations, this tool is easily incorporated in our envelope model, that is employed to derive the effective temperature of TP-AGB models during their quiescent inter-pulse evolution. In this way, we can follow the evolution of molecular opacities as more carbon is dredged-up to the surface, and in particular the abrupt change in the dominant opacity sources at the transition from the the oxygen- to the carbon-rich domain. Correspondingly, the most remarkable consequence is the sudden cooling of the stellar tracks in the $\log L - \log T_{\rm eff}$ diagram, which causes the displacement of the C-rich models towards redder near-infrared colours.

We expect that the latter effect should depend, among other factors, on the global metal content of the stellar population which the observed AGB stars belong to. Preliminary calculations suggest that the cooling of the C-rich models away from the O-rich AGB should be less pronounced at decreasing metallicity, possibly becoming even negligible in AGB populations of very low metallicity. This would occur if the temperatures across the atmosphere are too warm (say >4000 K, or equivalently for $\log T_{\rm eff} > 3.6$) and do not fall in the temperature range required for the formation of the characteristic molecules (e.g. CO, H_2O, and CN) in appreciable concentrations.

Furthermore, the results obtained in this work indicate that – while keeping fixed all other prescriptions – the adoption of more consistent molecular opacities in AGB models produces significant effects, such as: shortening of the C-star phase, lower AGB-tip luminosities and final masses for C-stars, lower carbon yields. Of course, all these aspects need to be investigated in the context of a more extended analysis that performs a re-calibration of the model parameters (e.g. the dredge-up law) to reproduce basic observables of C-stars (Marigo et al., in preparation).

It is also clear that the predicted evolution of the effective temperature as a function of the surface C/O ratio – shown in this study for AGB models with initial solar metallicity – should be considered representative of a mean trend, as it refers to quiescent inter-pulse stages. Additional effects – such as stellar pulsation (instead of the assumed staticity of the envelope), and the complex variation of the envelope structure (in terms of contraction and/or expansion) driven by thermal pulses – should produce some further dispersion around the mean $T_{\rm eff}$ at given C/O. Moreover, major improvements in the opacity treatment could be adopted in future work, including the resort to detailed opacity libraries as they may become available.

Anyhow, we expect that none of these additional elements could change the main point of this study: the large inadequacy of fixed solar-scaled molecular opacities in AGB models with varying C and O surface abundances, and the marked cooling of the AGB for C/O > 1.

Actually, a net progress in model predictions is already attained in the present analysis, as supported by the first successful comparisons with observations of e.g. C/O ratios, effective temperatures, and near-infrared colours of C-stars. This improvement in modelling the TP-AGB phase opens the way to promising applications, aimed at investigating the contribution of old- and intermediate-age stellar populations to the chemical and spectrophotometric evolution of the parent galaxies.

More realistic TP-AGB models are really needed to keep up with observational advancements: AGB stars have been resolved in many galaxies of the Local Group (see e.g. Nowotny et al. 2001; Saviane et al. 2000; Groenewegen 1999 for a recent census), and also indirectly revealed via their signature in the integrated spectra of the stellar systems (e.g. Lançon et al. 1999). Moreover, huge amounts of infrared data with unprecedented sky coverage are being released (e.g. the DENIS and 2MASS projects).

In this context, the issue addressed in this work should provide an important step forward to bring AGB stellar models closer to observations.

Acknowledgements. I would like to thank Harm Habing for fruitful suggestions and remarks on this work, and Léo Girardi for careful and critical reading of the manuscript. This work is financially supported by the Italian Ministry of Education, University and Research (MIUR).

References

Alexander, D. R., Johnson, H. R., & Rypma, R. L. 1983, ApJ, 272, 773
Alexander, D. R., Augason, G. C., & Johnson, H. R. 1989, ApJ, 345, 1014
Alexander, D. R., & Ferguson, J. W. 1994, ApJ, 437, 879
Bergeat, J., Knapik, A., & Rutily, B. 2001, A&A, 369, 178
Bessell, M., Brett, J. M., Scholz, M., et al. 1989, A&AS, 77, 1
Bessell, M., Brett, J. M., Scholz, M., et al. 1991, A&AS, 87, 621
Bessell, M. S., Castelli, F., & Plez, B. 1998, A&A, 331, 231
Brown, J. A., Johnson, H. R., Cutright, L. C., et al. 1989, ApJS, 71, 623
Chieffi, A., Domínguez, I., Limongi, M., et al. 2001, ApJ, 554, 1159
Cioni, M.-R., Loup, C., Habing, H. J., et al. 2000, A&AS, 144, 235
Costa, E., & Frogel, J. A. 1996, ApJ, 112, 2607
Fluks, M. A., Plez, B., Thé, P. S., et al. 1994, A&AS, 105, 311
Forestini, M., & Charbonnel, C. 1997, A&AS, 123, 241
Frogel, J. A., Mould, J. B., & Blanco, V. M. 1990, ApJ, 352, 96
Girardi, L., Bressan, A., Bertelli, G., & Chiosi, C. 2000, A&AS, 141, 371
Groenewegen, M. A. T. 1999, in Asymptotic Giant Branch Stars, ed. T. Le Bertre, A. Lebre, & C. Waelkens, IAU Symp., 191, 535
Gustafsson, B. 1995, in Astrophysical Applications of Powerful New Databases, ed. S. J. Adelman, & W. L. Wiese, ASP Conf. Ser., 78, 347
Gustafsson, B., & Jørgensen, U. G. 1994, A&AR, 6, 19
Habing, H. J. 1996, A&ARv, 7, 97
Herwig, F. 2000, A&A, 360, 952
Höfner, S., & Jørgensen, U. G., Loidl, R., et al. 1998, A&A, 340, 497
Iglesias, C. A., & Rogers, F. J. 1993, ApJ, 412, 752
Irwin, A. W. 1981, ApJS, 45, 621
Ivezić, Z., & Elitzur, M. 1995, ApJ, 445, 415
Johnson, H. R. 1982, ApJ, 260, 254
Jørgensen, U. G., Johnson, H. R., & Nordlund, A. 1992, A&A, 261, 263
Keeley, D. A. 1970, ApJ, 161, 643
Lambert, D. L., Gustafsson, B., Eriksson, K., & Hinkle, K. H. 1986, ApJS, 62, 373
Lançon, A., Mouhcine, M., Fioc, M., et al. 1999, A&A, 344, L21
Lançon, A., & Wood, P. R. 2000, A&AS, 146, 217
Loup, C., Forveille, T., Omont, A., et al. 1993, A&AS, 99, 291

Lucy, L. B., Robertson, J. A., & Sharp, C. M. 1986, A&A, 154, 267
Marigo, P. 1998, A&A, 340, 463
Marigo, P. 2001, A&A, 370, 194
Marigo, P., Bressan, A., & Chiosi, C. 1996, A&A, 313, 545
Marigo, P., Bressan, A., & Chiosi, C. 1998, A&A, 331, 564
Marigo, P., Girardi, L., & Bressan, A. 1999, A&A, 344, 123
Nowotny, W., Kerschbaum, F., Schwarz, H. E., et al. 2001, A&A, 367, 557
Ohnaka, K., & Tsuji, T. 1996, A&A, 310, 933
Ohnaka, K., Tsuji, T., & Aoki, W. 2000, A&A, 353, 528
Plez, B. 1992, A&AS, 94, 527
Portinari, L., Chiosi, C., & Bressan, A. 1998, A&A, 334, 505
Pottasch, S. R. 2000, in Asymmetrical Planetary Nebulae II: From Origins to Microstructures, ed. H. Kastner, N. Soker, & S. Rappaport, ASP Conf. Ser., 199, 289
Querci, F., Querci, M., & Kunde, V. G. 1971, A&A, 15, 256
Querci, F., Querci, M., & Tsuji, T. 1974, A&A, 31, 265
Rossi, S. C. F., & Maciel, W. J. 1983, Ap&SS, 96, 205
Russell, H. N. 1934, ApJ, 79, 317
Sauval, A. J., & Tatum, J. B. 1984, ApJS, 56, 193
Saviane, I., Held, E. V., & Bertelli, G. 2000, A&A, 355, 56
Scalo, J. M., & Ulrich, R. K. 1975, ApJ, 200, 682
Sergei, N., & Weinberg, M. D. 2000, ApJ, 542, 804
Smith, V., & Lambert, D. L. 1985, ApJ, 294,326
Smith, V., & Lambert, D. L. 1986, ApJ, 311, 843
Smith, V., & Lambert, D. L. 1990, ApJS, 72, 387
Tsuji, T. 1966, PASJ, 18, 127
van der Veen, W. E. C. J., & Habing, H. J. 1988, A&A, 194, 125
Vassiliadis, E., & Wood, P. R. 1993, ApJ, 413, 641
Ventura, P., D'Antona, F., & Mazzitelli, I. 1999, ApJ, 524, L111
Wannier, P. G., Sahai, R., Andersson, B-G., et al. 1990, ApJ, 358, 251
Wood, P. R. 1981, in Physical processes in red giants, Proc. of the Second Workshop, Erice, Italy (September 3–13, 1980) (Dordrecht, D. Reidel Publishing Co.), 135